JOURNAL OF GEOPHYSICAL RESEARCH, VOL. 114, D18204, doi:10.1029/2009JD011773, 2009

Cloud influence on and response to seasonal Arctic sea ice loss

Jennifer E. Kay[1,2] and Andrew Gettelman[1]

Received 20 January 2009; revised 24 June 2009; accepted 2 July 2009; published 19 September 2009.

[1] Recent declines in Arctic sea ice extent provide new opportunities to assess cloud influence on and response to seasonal sea ice loss. This study combines unique satellite observations with complementary data sets to document Arctic cloud and atmospheric structure during summer and early fall. The analysis focuses on 2006–2008, a period over which ice extent plummeted to record levels, substantial variability in atmospheric circulation patterns occurred, and spaceborne radar and lidar observations of vertical cloud structure became available. The observations show that large-scale atmospheric circulation patterns, near-surface static stability, and surface conditions control Arctic cloud cover during the melt season. While no summer cloud response to sea ice loss was found, low clouds did form over newly open water during early fall. This seasonal variation in the cloud response to sea ice loss can be explained by near-surface static stability and air-sea temperature gradients. During summer, temperature inversions and weak air-sea temperature gradients limit atmosphere-ocean coupling. In contrast, relatively low static stability and strong air-sea gradients during early fall permit upward turbulent fluxes of moisture and heat and increased low cloud formation over newly open water. Because of their seasonal timing, cloud changes resulting from sea ice loss play a minor role in regulating ice-albedo feedbacks during summer, but may contribute to a cloud-ice feedback during early fall.

Citation: Kay, J. E., and A. Gettelman (2009), Cloud influence on and response to seasonal Arctic sea ice loss, *J. Geophys. Res.*, *114*, D18204, doi:10.1029/2009JD011773.

1. Introduction

[2] Arctic sea ice extent is declining at impressive rates, especially during summer and early fall. One scientific opportunity that emerges from this dramatic decline is the ability to observationally assess the processes responsible for seasonal sea ice loss. In this study, we document and explain recent variations in Arctic cloud patterns and vertical structure. We then assess the influence of clouds on seasonal Arctic sea ice loss.

[3] In the Arctic, herein defined as poleward of 65°N, many factors affect cloud formation and evolution. These factors include the large-scale atmospheric circulation, boundary layer structure, surface properties, absorption and emission of radiation, microphysical processes, and aerosol forcing. The relative importance of these factors changes both geographically and seasonally, as might be expected in an environment that experiences large variations in climatic conditions. The complexity of Arctic cloud processes and the seasonal cycle of Arctic cloud radiative forcing have been explored in previous studies [e.g., *Curry et al.*, 1996; *Intrieri et al.*, 2002]. Here a brief overview of the salient controls and uncertainties is provided to motivate and provide context for the observations analyzed in this study.

[4] Large-scale atmospheric circulation patterns produce the temperature and moisture conditions that govern Arctic cloud processes. Wind patterns control the transport of heat and moisture in and around the Arctic, and thus have a primary influence on Arctic clouds. For example, large-scale dynamics influence cloud formation and evolution within frontal systems. In the winter, cyclones primarily occur in the North Atlantic storm track, where storm activity peaks near the mean Icelandic Low and extends northeastward into the Barents Seas. During summer, Arctic cyclone activity peaks over the central Arctic Ocean resulting from storms that form over the Eurasian continent and the Arctic Ocean [*Serreze and Barrett*, 2008]. While frontal systems at times dominate Arctic cloud production, many Arctic clouds are not directly associated with active cyclones. Of particular significance are Arctic low clouds (cloud top height <3 km), which have a large influence on the Arctic surface energy budget.

[5] Arctic low cloud formation and evolution occurs in both stable and unstable atmospheres [*Curry et al.*, 1996]. In stable atmospheres, stratus or fog layers form when warm and moist air overlies a relatively cold surface. If cooling allows the air mass relative humidity to reach saturation, low cloud formation ensues. Once a cloud forms, it can maintain itself and create vertical mixing through cloud top radiative cooling [e.g., *Herman and Goody*, 1976; *Morrison and Pinto*, 2005; *Pinto*, 1998]. Even if a cloud-topped

[1]Climate and Global Dynamics, National Center for Atmospheric Research, Boulder, Colorado, USA.
[2]Department of Atmospheric Sciences, Colorado State University, Fort Collins, Colorado, USA.

0148-0227/09/2009JD011773$09.00

mixed layer results, turbulent surface-atmosphere coupling is often limited by temperature inversions. Warm air advection from lower latitudes often provides conditions suitable for cloud formation via the warm air advection mechanism (e.g., summer Arctic stratus clouds discussed by *Herman and Goody* [1976], autumnal mixed-phase clouds discussed by *Pinto* [1998]). Arctic low clouds also form in unstable environments when cool air overlies a relatively warm surface. Under this scenario, an unstable boundary layer permits strong surface-atmosphere coupling via upward moisture and heat fluxes. Cloud formation in unstable environments can lead to open cell convection or banded roll convection in which buoyant cloudy plumes are interspersed with regions of subsidence (e.g., winter roll clouds in the Bering Sea discussed by *Walter* [1980]). High-resolution modeling shows that open water facilitates the convective development of cold-air outbreak roll clouds [*Liu et al.*, 2006]. In the North Atlantic, cold air advection across strong sea surface temperature gradients associated with the Gulf Stream leads to low clouds via this process. Buoyancy-driven clouds also occur when a typically ice-covered ocean becomes open water. A prime example of this phenomenon are lead clouds, which form due to large turbulent fluxes associated with up to 40 K air-sea temperature differences. Another example are clouds forming over open water in the early fall when the atmosphere temperature decreases faster than the open ocean temperature and/or cold airflows off ice over relatively warm open water.

[6] Arctic low clouds are different than their low latitude cousins, the subtropical stratocumulus. *Klein and Hartmann* [1993] used observations to demonstrate that when subsidence increases in the subtropical highs, the boundary layer height decreases, and low cloud cover increases. Yet *Klein and Hartmann* [1993] note that seasonal changes in Arctic low clouds do not follow this simple rule, possibly because of the large seasonal changes in the boundary layer temperature structure and stability. For example, the presence of a strong surface inversion is common in the Arctic, but uncommon in the subtropics. In the stratocumulus regimes, cloud top radiative cooling drives low cloud formation, while surface buoyant fluxes of latent and sensible heat play a secondary role. Cloud top radiative cooling is also of primary importance for maintaining Arctic clouds; however, surface fluxes and horizontal advection can also be primary driving factors for Arctic low clouds [e.g., *Klein et al.*, 2009].

[7] Although the basic mechanisms for Arctic cloud formation and evolution have been outlined, many questions remain. Unresolved problems in understanding Arctic clouds are primarily associated with microphysical processes, cloud-aerosol interactions, and cloud-sea ice interactions. Vertical cloud and temperature information from NASA's A-train satellite constellation provide new motivation to investigate these outstanding gaps in our understanding of Arctic cloud processes [e.g., *Kay et al.*, 2008]. Until recently, accurate and continuous observations of Arctic vertical cloud structure have occurred at a limited number of sites confined to the Arctic coastline (e.g., from the cloud radars and lidars at Barrow and Eureka described in *de Boer et al.* [2009]). In this study, we combine A-train satellite data with complementary data sets to assess relationships between recent summer and early fall cloudiness and factors such as sea ice extent, boundary layer structure, and large-scale atmospheric circulation variability. In particular, the observations are leveraged to evaluate evidence for cloud changes resulting from recent Arctic sea ice loss, herein termed a "cloud response to sea ice loss".

[8] Previous observations and modeling studies provide physical insight into the anticipated cloud response to sea ice loss. For example, one candidate for a cloud response is an increase in low clouds over newly open water. This response might be expected in the fall when the surface and the atmosphere are coupled by turbulent fluxes. Indeed, cloud over open water and not over sea ice has been observed in the marginal ice zone during fall and winter [e.g., *Paluch et al.*, 1997; *Brummer*, 1996]. On the other hand, the summer low cloud response to sea ice loss might be small because clouds are often decoupled from the underlying surface [*Herman and Goody*, 1976]. A frontal cloud response to sea ice loss could also occur because the sea ice margin enhances low-level baroclinicity [e.g., *Tsukernik et al.*, 2007]. *Deser et al.* [2000], *Alexander et al.* [2004], and *Deser et al.* [2004] all find evidence for winter atmospheric circulation responses to observed sea ice loss that could in turn influence cloud cover. The atmospheric circulation response to projected sea ice loss [*Deser et al.*, 2009; *Higgins and Cassano*, 2009] will contribute to the future cloud response to sea ice loss. Although previous work guides expectations for the physical processes controlling a cloud response to sea ice loss, the influence of vast expanses of open water during late summer and early fall on Arctic clouds has never been observed.

2. Methods

[9] To document ocean, atmospheric, and cloud conditions, we compiled data from a number of sources. Our analysis focused on 2006 through 2008, but data from earlier years were used to place these years in context. Analysis was limited to summer ("JJA", June, July, August) and early fall ("SO", September, October).

[10] We assessed Arctic Ocean conditions with sea ice extent and sea surface temperatures data sets. Passive microwave satellite observations have been used to document Arctic sea ice loss [e.g., *Serreze et al.*, 2007] and enabled quantification of sea ice extent for this study. Available from June 1979 to present, NIMBUS-7 SMMR and DMSP SSM/I passive microwave data provide hemispheric estimates of ice extent [*Meier et al.*, 2006; *Cavalieri et al.*, 1996]. Available from June 2002 to present, AMSR-E passive microwave data have higher resolution than SMMR and SSM/I (12.5 km versus 25 km) and allow detailed mapping of sea ice concentrations in recent years [*Cavalieri et al.*, 2004]. Data from *Hurrell et al.* [2008] were used to document sea surface temperatures.

[11] Satellite and atmospheric reanalysis were utilized to analyze atmospheric conditions. V4 Atmospheric Infrared Sounder (AIRS) data [*Gettelman et al.*, 2006] and radiosonde observations from the Barrow, Alaska Atmospheric Radiation Measurement site [*Stamnes et al.*, 1999] enabled assessment of seasonal changes in near-surface static stability and near-surface temperatures. Although AIRS retrievals are sensitive to cloud cover, *Gettelman et al.* [2006] showed that AIRS retrievals in polar regions are unbiased relative to in situ radiosondes. AIRS temperature detection for 1 km layers

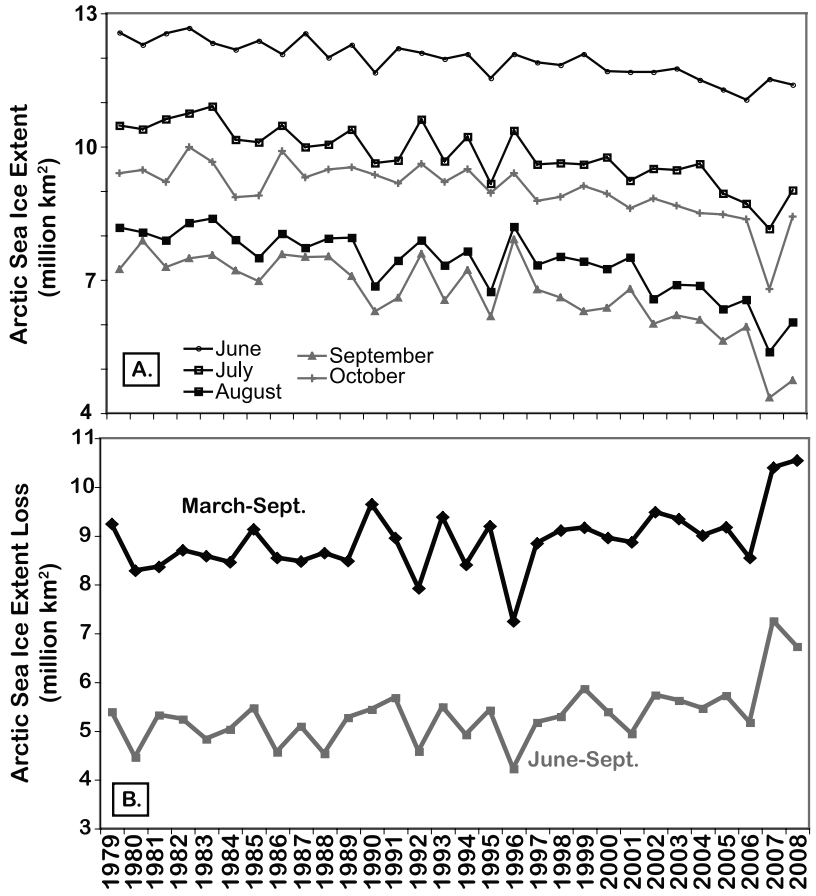

Figure 1. Arctic sea ice extent and seasonal ice extent loss. (a) Time series of monthly mean Arctic sea ice extent. (b) Time series of Arctic sea ice extent loss during the entire melt season (March monthly mean minus September monthly mean) and during the summer melt season (June monthly mean minus September monthly mean). Sea ice extents are from NIMBUS-7 SMMR and DMSP SSM/I passive microwave data.

has an accuracy of approximately 1°C [*Divakarla et al.*, 2006]. Because of the course vertical resolution of AIRS, broad changes in temperature structure can be assessed, but the detailed inversion structure that often controls atmosphere-ocean coupling cannot be detected. Large-scale atmospheric circulation patterns were examined using the NCAR/NCEP reanalysis (NRA [*Kalnay et al.*, 1996]). Only sea level pressure (SLP) and free tropospheric temperature fields were utilized, as these are among the more reliable fields from data-poor reanalysis models in the Arctic.

[12] Data from colocated spaceborne radar and lidar, CloudSat and Cloud-Aerosol LIdar with Orthogonal Polarization (CALIOP), were used to document cloud patterns on seasonal timescales and to examine relationships between cloud vertical structure, atmospheric conditions, and sea ice cover [*Stephens et al.*, 2008]. CloudSat and CALIOP data are particularly valuable in polar regions because their cloud detection technique does not rely on thermal or albedo contrast, but instead on the return of an active pulse.

[13] The influence of radar sensitivity, radar surface clutter, and lidar attenuation on cloud detection is important to disclose. CloudSat's minimum detectable radar reflectivity is approximately ~ -29 dBZ, which will prevent detection of clouds that are optically thin and/or dominated by small particles. Due to a strong surface return, CloudSat data below $\sim$720 m are contaminated and cloud detection is difficult. Fortunately, *de Boer et al.* [2009] found that CloudSat's sensitivity (surface clutter) only prevents detection of 7% (10%) of the single-layer mixed-phase Arctic clouds over 2.5 years at Eureka, Canada. Column cloudiness causes significant lidar attenuation and is especially problematic for cloud detection under optically thick clouds. When optically thick clouds overlie low clouds occurring below $\sim$720 m, both CloudSat and CALIOP will be unable to detect them.

[14] Two CloudSat standard products, R04 2B-GEOPROF [*Marchand et al.*, 2008] and P1.R04 2B-GEOPROF-LIDAR [*Mace et al.*, 2009] were combined to create CloudSat + CALIOP cloud masks with a vertical resolution of 240 m. Because attenuation is not identified in the 2B-GEOPROF-LIDAR product, we only use data above 720 m where radar data enable discrimination between clear and attenuated lidar observations. CALIOP Level 2 Vertical Feature Mask (VFM) data with a vertical resolution of 60 m were also used to assess cloud changes. The CALIOP VFM data are particularly valuable for assessing changes in low (<720 m) and geometrically thin cloud cover.

[15] Passive radiometer cloud observations were also analyzed to complement the CloudSat and CALIOP cloud observations. We evaluated Moderate Resolution Imaging

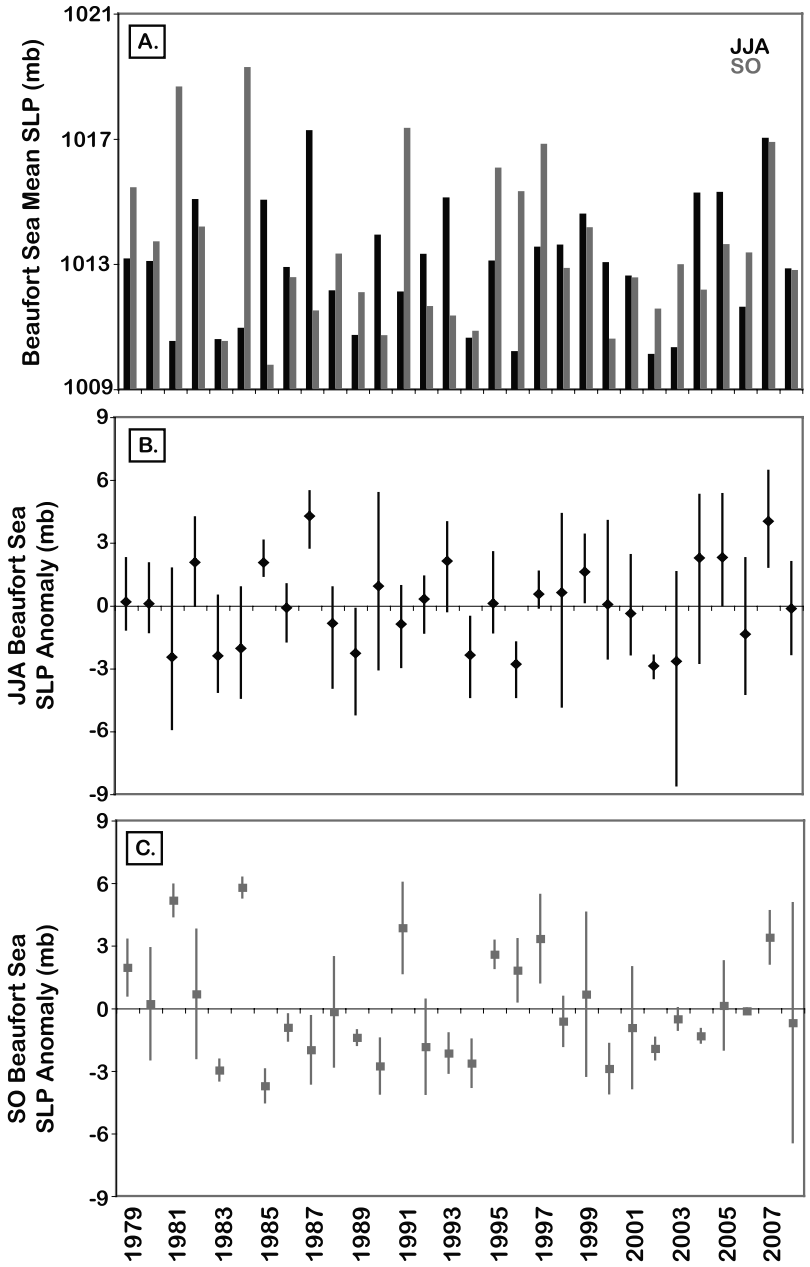

Figure 2. Time series (1979–2008) of summer (JJA) and early fall (SO) Sea Level Pressure (SLP) in the Beaufort Sea. (a) Mean SLP. (b) JJA SLP anomaly. (c) SO SLP anomaly. Whiskers in Figures 2b and 2c show the seasonal range in monthly SLP anomaly. SLP data are from the NRA.

Spectroradiometer (MODIS) radiance-based threshold estimates of cloud cover (Cloud_Fraction_Combined Level-3, collection 5 product, see *Platnick et al.* [2003]) from both the Terra and Aqua satellite platforms, but because of their similarity, only data from MODIS Aqua are presented. We also examined cloud estimates from Multiangle Imaging SpectroRadiometer (MISR) (Version 1.0, ''Cloud_Fraction_NN'' [*Di Girolamo et al.*, 2009]). MISR is a part of Terra, but the similarity between MODIS Terra and Aqua cloud amounts suggest that cloud cover differences related to overpass timing are small. MISR cloud detection is accomplished through radiance-based thresholding [*Zhao and Di Girolamo*, 2004], angular signatures [*Di Girolamo and Wilson*, 2003], and stereoscopic [*Moroney et al.*, 2002] methods. MODIS and MISR both have better spatial sampling than CloudSat + CALIOP, and are thus useful for examining monthly variations in cloud cover; however, MODIS and MISR cloud retrieval algorithms have limitations resulting from their need to discriminate between radiance from the surface and the overlying atmosphere, and their use of surface data sets that can bias cloud retrievals. Because the MODIS and MISR retrieval algorithms rely on solar radiation, retrieval quality declines in early fall when there is limited solar radiation and solar zenith angles are large. For this reason, MODIS and MISR data are only used through September.

[16] Given the diverse cloud detection methods utilized by CloudSat, CALIOP, MODIS, and MISR, differences in

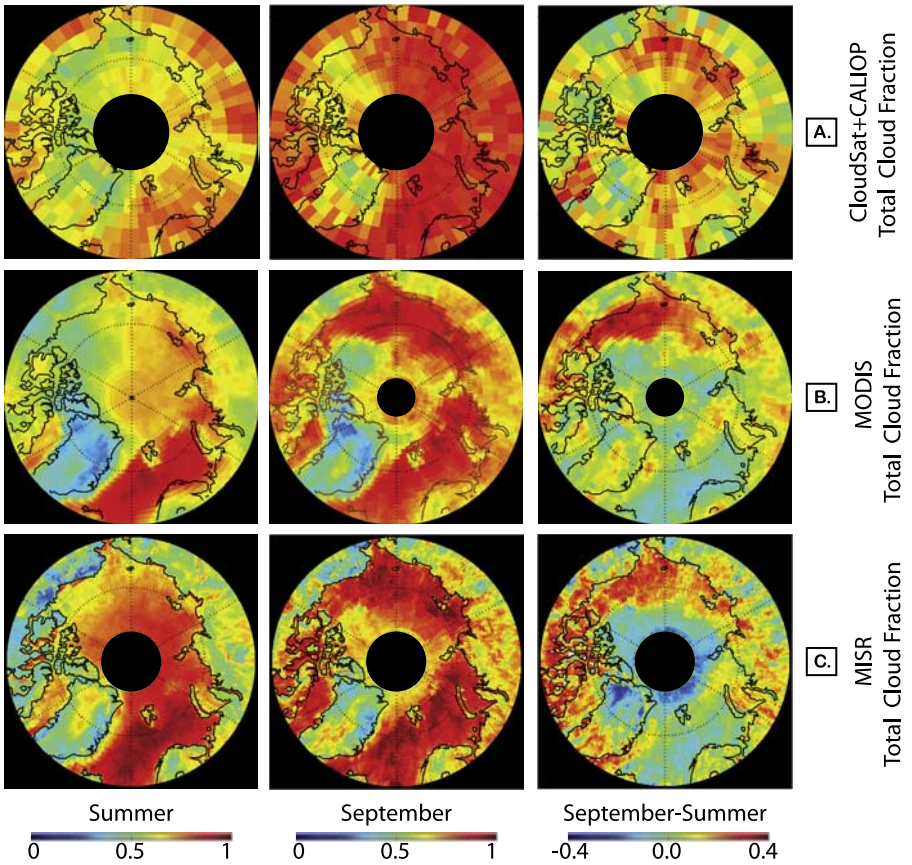

Figure 3. Summer (JJA) and September total cloud maps. (a) CloudSat + CALIOP total cloud fraction. Columns are cloudy if the total cloud thickness detected by CloudSat + CALIOP exceeds 960 m (4 bins). (b) MODIS total cloud fraction. (c) MISR total cloud fraction. All plots show 2006–2008 average values.

retrieved Arctic cloud properties are expected. While we discuss obvious differences, we do not fully diagnose their underlying causes, which are related both to instrument sensitivity and to cloud retrieval methods. Instead, we emphasize relationships between cloud cover, atmospheric circulation patterns, and the surface state that are found in all four data sets. We assume that confidence in the assessed relationships is merited when consistency between the data sets is found.

3. Results

3.1. Long-term Context for the 2006 Through 2008 Sea Ice and Atmospheric Circulation Patterns

[17] Changing sea ice and atmospheric conditions from 2006 through 2008 provide a natural laboratory to document and understand the physical controls on Arctic clouds. Although this analysis relies on a short time period, unprecedented sea ice loss, and significant variability in Arctic atmospheric circulation patterns occurred during these three years.

[18] Passive microwave sea ice observations show Arctic sea ice extent is declining, especially in the late summer (Figure 1). The past two years, 2007 and 2008, had impressive ice extent minima and extent loss over the melt season [*Stroeve et al.*, 2008]. During 2007, sea ice extent set record-low monthly values from July through October. 2007 also had the largest summer ice loss (September ice extent minus June ice extent) on record. Monthly mean Arctic sea ice extents in 2008 were the second lowest on record from August through September. More impressively, 2008 had the largest ice extent loss over an entire melt season (September ice extent minus March ice extent) due to relatively extensive ice in March 2008. 2008 also had the largest September to October ice extent increase ever recorded. Although sea ice extents during 2006 were far below long-term mean values, ice extent loss over the 2006 melt season was not anomalous. Thus 2006 provides a useful contrast to the record-low sea ice conditions present during 2007 and 2008.

[19] The Beaufort High is an important feature of large-scale atmospheric circulation variability in the Arctic, and has a strong influence on summer and early fall sea ice extent variability [*Ogi and Wallace*, 2007]. Indeed, the thermodynamic and dynamic forcing associated with the strong Beaufort High during the 2007 melt season has been documented as a key factor for explaining the record-breaking 2007 ice extent minimum [e.g., *Stroeve et al.*, 2008; *Kay et al.*, 2008; *Zhang et al.*, 2008; *Perovich et al.*, 2008]. One measure of the Beaufort High is the NRA SLP in the Beaufort Sea. The mean and anomaly of this metric reveals the strong and persistent Beaufort High during summer and early fall 2007 (Figure 2). The persistent sign and strength of the Beaufort High during the 2007 melt season is unprecedented over the 1979–2008 period. The physical mechanism for this persistent circulation anomaly

Table 1. CloudSat + CALIOP Arctic Cloud Fractions

Region	Cloud Type[a]	JJA	SO	SO-JJA
65–82°N	total cloud (dz > 960 m)	64%	78%	14%
	total cloud (dz > 480 m)	77%	86%	9%
	low cloud	59%	76%	17%
	unique low cloud	27%	33%	6%
	low cloud/total cloud (dz > 480 m)	76%	88%	12%
	unique low cloud/low cloud	46%	43%	−3%
Beaufort Sea (125–156°W 70–76°N)	total cloud (dz > 960 m)	53%	71%	18%
	total cloud (dz > 480 m)	66%	86%	20%
	low cloud	45%	76%	31%
	unique low cloud	20%	41%	21%
	low cloud/total cloud (dz > 480 m)	68%	89%	21%
	unique low cloud/low cloud	45%	54%	9%
Chukchi Sea (156–180°W 70–76°N)	total cloud (dz > 960 m)	57%	84%	27%
	total cloud (dz > 480 m)	71%	94%	23%
	low cloud	51%	88%	38%
	unique low cloud	24%	46%	21%
	low cloud/total cloud (dz > 480 m)	71%	94%	23%
	unique low cloud/low cloud	48%	52%	4%
East Siberian Sea (145–180°E 70–76°N)	total cloud (dz > 960 m)	62%	85%	23%
	total cloud (dz > 480 m)	77%	93%	16%
	low cloud	57%	87%	30%
	unique low cloud	28%	35%	6%
	low cloud/total cloud (dz > 480 m)	74%	93%	19%
	unique low cloud/low cloud	50%	40%	−10%
GIN Seas (66–76°N 20 W–15°E)	total cloud (dz > 960 m)	68%	85%	17%
	total cloud (dz > 480 m)	84%	92%	7%
	low cloud	72%	84%	12%
	unique low cloud	38%	39%	0%
	low cloud/total cloud (dz > 480 m)	85%	92%	7%
	unique low cloud/low cloud	53%	46%	−8%

[a]The definitions of low and unique low cloud are the same as in Figure 4.

remains unexplained. *L'Heureux et al.* [2008] investigated mechanisms for this circulation anomaly, and found that it was not a response to emerging La Nina conditions. In contrast to 2007, the Beaufort High in 2006 was relatively weak in JJA and average in SO, while in 2008 the Beaufort High had near-average strength in both JJA and SO.

[20] Given this context for recent Arctic sea ice and atmospheric circulation patterns, we next present average cloud and near-surface atmospheric conditions during the 2006 through 2008 period. The average conditions provide a means to compare the satellite data sets, and to present useful background for the year-to-year variability that is discussed later.

3.2. Average Arctic Cloud Patterns and Atmospheric Temperature Structure

3.2.1. Average Cloud Patterns During 2006–2008

[21] The satellite data sets reveal seasonal variations in the spatial patterns of total Arctic cloud cover from summer to September (Figure 3). All three data sets show a summer cloud maximum over the Greenland, Icelandic, and Norwegian (GIN) seas (centered at 0°W, 72°N) with relatively fewer clouds over Greenland (centered at 40°W, 72°N), the Canadian Archipelago (centered at 100°W, 75°N) and the Beaufort Sea (centered at 140°W, 73°N). In the Pacific sector, including the marginal seas from the Laptev Sea (centered at 125°E, 76°N) East to the East Siberian Sea (centered at 162°W, 72°N), the Chukchi Sea (centered at 168°W, 72°N), and the Beaufort Sea, all data sets detect large increases in cloudiness from summer into early fall.

[22] Although the three cloud data sets have many similarities, there are also several significant disagreements in retrieved cloud amount and pattern. First, CloudSat + CALIOP detect many more clouds over land than MODIS or MISR. As a result, the cloud contrast between the open ocean and nearby land regions is much greater in the MODIS and MISR data than in the CloudSat + CALIOP data. Second, MISR detects more JJA clouds than CloudSat + CALIOP or MODIS over the central Arctic Ocean (Figure 3). The additional summer clouds that MISR detects are geometrically thin clouds below 1 km. Finally, the September-JJA maps highlight spatial pattern differences. MISR shows cloud decreases from JJA into September at high latitudes, whereas CloudSat + CALIOP show cloud increases and MODIS shows little change. MISR and MODIS also show larger increases in cloudiness over Northern Canada from JJA to September than CloudSat + CALIOP. Finally, CloudSat + CALIOP have relatively sparse sampling when compared to MODIS and MISR, resulting in relatively noisy CloudSat + CALIOP spatial distributions.

[23] Discrepancies in the total cloud amount detected by CloudSat + CALIOP, MODIS, and MISR are expected. They result from differing cloud detection techniques and instrument sensitivities. Although differences in detected cloud amount are informative, they cannot be used for quantitative comparisons or validation. For example, we calculated CloudSat + CALIOP total cloud cover using two vertically integrated cloud thickness thresholds: 480 m and 960 m. Over the entire Arctic region observed by CloudSat + CALIOP (65–82 N), this increase in the applied cloud thickness threshold decreased total cloud amount by 13% in JJA and by 8% in SO (Table 1). In other words, the thickness threshold that was selected for cloud detection had an appreciable impact on the total detected

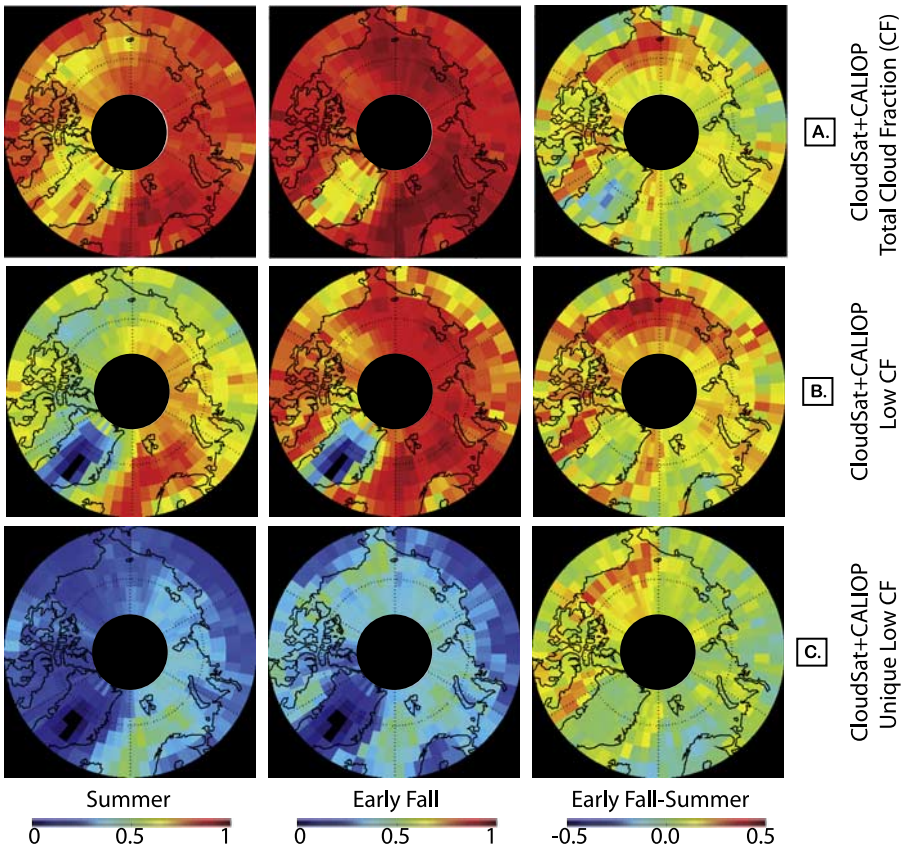

Figure 4. CloudSat + CALIOP summer (JJA) and early fall (SO) total and low cloud maps. (a) Total Cloud Fraction. Columns are cloudy if the total cloud thickness detected by CloudSat + CALIOP exceeds 480 m (2 bins). (b) Low Cloud Fraction. Columns contain low clouds if the cloud thickness below 3 km ASL detected by CloudSat + CALIOP exceeds 480 m (2 bins). (c) Unique Low Cloud Fraction. Profiles were classified as having unique low clouds if low clouds were the only clouds detected in the column. All plots show 2006–2008 average values.

cloud amount. This simple sensitivity test highlights the importance of using a consistent cloud definition when making quantitative cloud amount comparisons between observational data sets [e.g., *Ackerman et al.*, 2008], and between observations and models [e.g., *Bodas-Salcedo et al.*, 2008].

[24] CloudSat + CALIOP data reveal the occurrence and distribution of low-level clouds during summer and early fall (Figure 4, Table 1). Over the entire Arctic area observed by CloudSat + CALIOP, low clouds (<3 km) made up a substantial fraction of total cloud cover: 76% in JJA and 88% in SO. Over the ocean, the spatial distribution of low cloud cover and total cloud cover were similar. During JJA, low cloud cover was greatest in the North Atlantic over the Greenland-Icelandic-Norwegian (GIN) Seas, but decreased from this region eastward to the Beaufort Sea. Low cloud cover increased from JJA to SO, especially over the Pacific marginal seas, including the Beaufort Sea (+31%), the Chukchi Sea (+38%), and the East Siberian Sea (+30%).

[25] Approximately half of the low clouds identified by CloudSat + CALIOP were unique (the only clouds in the column), indicating the frequent presence of thick and multilayer clouds. Like low clouds, unique low clouds increased from JJA to SO over the Pacific marginal seas. JJA to SO unique low cloud increases were greatest over the Chukchi Sea (+21%) and the Beaufort Sea (+21%), but smaller over the East Siberian Sea (+6%). In contrast, unique low-level cloud amounts did not increase from JJA to SO over the GIN seas. Because thick or multilayer clouds overlie many low clouds in the Arctic, signal attenuation presents a significant limitation for low cloud detection by the lidar.

3.2.2. Average Near-Surface Static Stability and Air Temperatures During 2006–2008

[26] Large seasonal and spatial variations in near-surface static stability and air temperatures are evident in soundings available from radiosonde and AIRS satellite observations (Figure 5). Near Barrow, both radiosonde and AIRS observations show decreasing near-surface static stability from June through October (Figure 5a). Although quantitative agreement is not expected due to differences in temporal sampling and vertical resolution, we do note that the radiosonde data have a larger seasonal contrast in static stability than the AIRS data. During summer, Barrow radiosonde and AIRS data (not shown) confirm previous analyses showing that near-surface air temperatures during summer are largely above freezing and thus the majority of summer low clouds are liquid (Figure 5b). In contrast, fall air temperatures are often below 0°C and mixed-phase low clouds are possible.

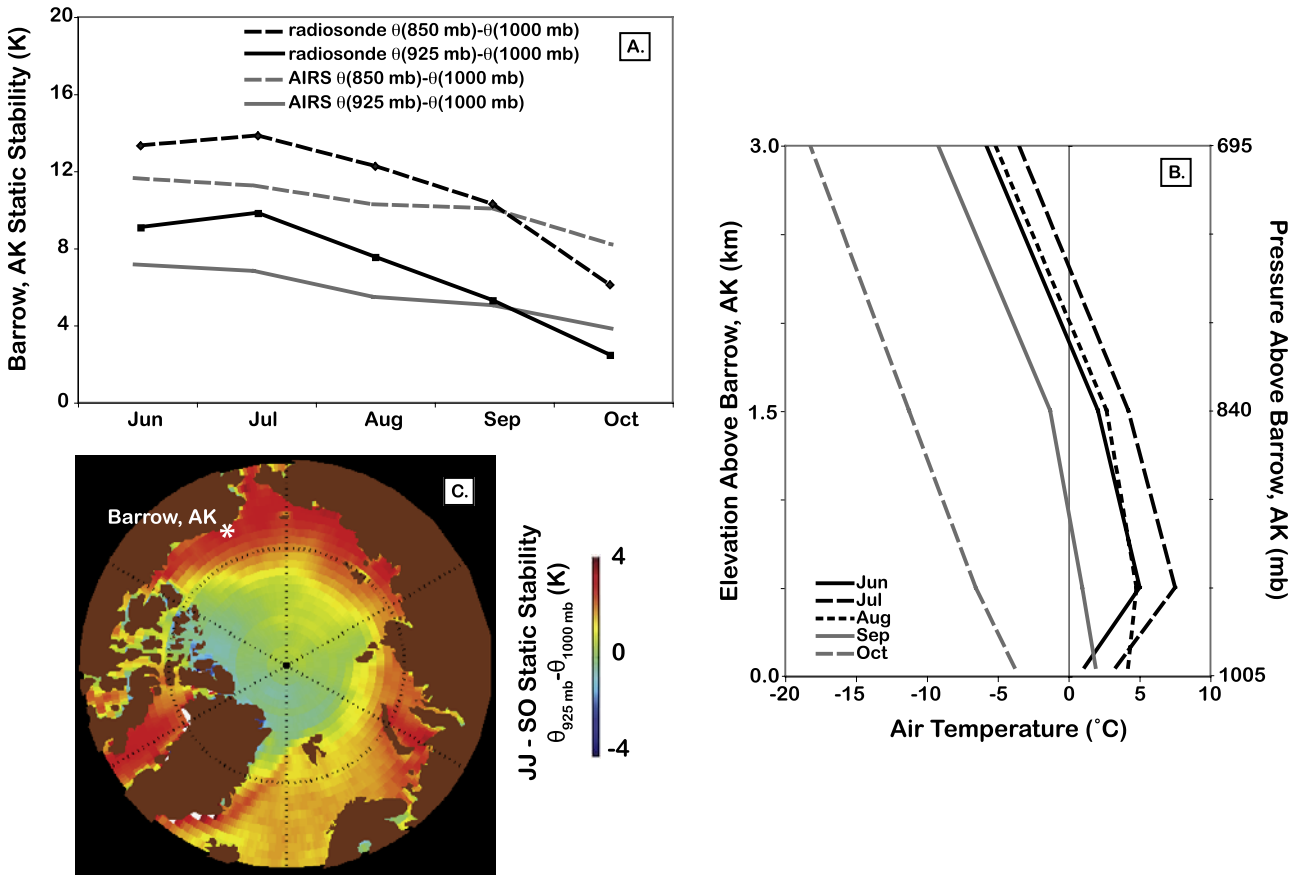

Figure 5. Arctic air temperatures and near-surface static stability. (a) Barrow, AK boundary layer static stability from radiosonde observations and AIRS (70–71°N, 156–157°W) data. (b) Barrow, AK monthly averaged air temperature profiles from radiosonde observations. (c) June + July minus September + October AIRS near-surface static stability. All plots show 2006–2008 average values.

[27] Qualitative agreement between Barrow radiosonde and AIRS observations provides increased confidence in using the AIRS data to evaluate spatial and temporal changes in air temperature and static stability throughout the Arctic. AIRS data show summer-to-early fall reductions in the near-surface static stability in the marginal seas, but slight summer-to-early fall static stability increases over the central Arctic (Figure 5c). In early fall, the atmosphere over the marginal seas has the lowest near-surface static stability in the annual cycle (not shown).

[28] In addition to near-surface static stability, we examined air-sea temperature gradients over the Pacific marginal seas (145°E to 125°W) during 2006–2008 using AIRS 1000 mb temperatures and the *Hurrell et al.* [2008] sea surface temperature data set. Average air-sea temperature gradients were weak in June, July, and August; open water temperatures were within 2 K of overlying 1000 mb air temperatures. In contrast, average September and October open water temperatures exceeded the average overlying 1000 mb air temperatures by 5 and 12 K respectively. Taken together, the near-surface static stability and air-sea temperature gradient observations demonstrate that the potential for atmosphere-ocean coupling in the Pacific marginal seas is greater in the early fall than in the summer.

[29] With some perspective on mean 2006–2008 Arctic atmospheric conditions and the strengths and weaknesses of the utilized data sets, we next present the year-to-year variability in Arctic sea ice extent, large-scale atmospheric circulation patterns, near-surface air temperature structure, and clouds from 2006 through 2008.

3.3. Summer (JJA) Year-to-Year Variability

3.3.1. Atmospheric and Sea Ice Conditions During Summer

[30] Significant variability in summer (JJA) large-scale atmospheric circulation patterns, near-surface static stability, and sea ice extent occurred from 2006 through 2008 (Figure 1, Figure 2, Figure 6). Of the three years, 2006 had the most extensive sea ice and the lowest Arctic-wide SLP. The mean 2006 JJA circulation had low pressure centered over the North Pole flanked by high pressure above Alaska/Northern Canada and Northern Europe, and low pressure over Siberia and Eastern Canada. The mean SLP pattern resulted in northwesterly winds in the Pacific sector that were favorable for ice extent maintenance. Air temperatures were lower than normal over the North Pole and Alaska, but slightly high or normal over the rest of the Arctic. AIRS observations suggest that the near-surface static stability was relatively normal, except near the pole where static stabilities were relatively low when compared to 2007 and 2008.

[31] During summer 2007, historically low sea ice extent occurred in the Pacific sector, especially in the East Siberian

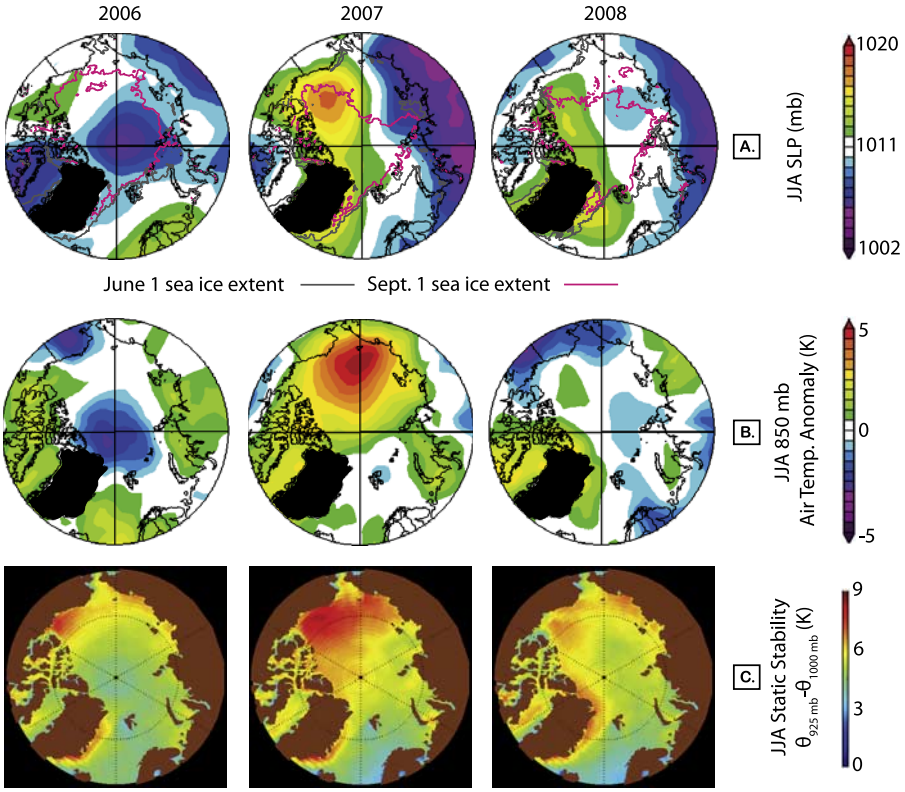

Figure 6. Year-to-year variability in summer (JJA) atmospheric conditions from 2006 to 2008. (a) NRA sea level pressure with sea ice extent contours based on AMSR-E 15% ice concentration line. (b) NRA 850 mb air temperature anomalies (from 1979–1995 mean). (c) AIRS near-surface static stability.

Sea. Associated with the strong Beaufort High (Figure 2), the mean 2007 JJA circulation pattern had a strong SLP gradient from North American to Northern Eurasia spanning the entire Arctic basin. Southerly winds associated with this SLP gradient pushed ice into the central Arctic and created up to +5°C 850 mb air temperature anomalies in the Pacific sector. Warm air advection aloft produced by the southerly winds also enhanced near-surface static stability over the Pacific marginal seas.

[32] Summer 2008 sea ice extent was the second lowest on record, despite relatively "benign" atmospheric circulation anomalies (Figure 2). Although there was less extensive ice loss in the East Siberian Sea and Central Arctic Ocean during 2008 as compared to 2007, there was more ice extent loss in the Beaufort Sea. During 2008, the mean JJA SLP patterns had high pressure flanking Greenland and Eastern Canada and low pressure over Western Canada/Alaska and Northern Eurasia. A strong Beaufort High set up in the late spring/early summer, but by late summer, low pressure dominated. Reflecting the variable large-scale circulation patterns, 850 mb air temperatures anomalies over the Arctic ocean were small and JJA 2008 static stability patterns were more similar to 2006 than to 2007.

3.3.2. Cloud Patterns and Vertical Structures During Summer

[33] Summer total cloud pattern anomalies reflected the year-to-year variability in large-scale atmospheric circulation patterns (Figure 7). Cloud reductions were associated with high pressure and anticyclonic circulation patterns, while cloud increases were associated with low pressure and cyclonic circulation patterns. The largest JJA cloud anomaly evident from 2006 through 2008 was the negative cloud anomaly associated with the strong Beaufort High during 2007. The 2007 cloud reductions were greatest in the CloudSat + CALIOP data and smallest in the MISR data. Cloud anomaly amplitude differences could result because MISR detects more JJA clouds over the ocean than CloudSat + CALIOP or MODIS (Figure 3). CloudSat + CALIOP measured cloud reductions West into the East Siberian Sea, while MODIS and MISR showed little cloud change or slight cloud increases West of the dateline. The 2006 and 2008 data also reveal cloud anomalies associated with SLP anomalies. During 2006, there were more clouds over the Arctic Ocean poleward of Canada associated with relatively low SLP. Northern Canada had fewer clouds during 2006 than during 2007 and 2008. All three data sets, but especially MODIS and MISR, had negative cloud anomalies along the Northern Siberia coastline (e.g., in the Laptev Sea) and Southwestern Greenland associated with relatively high SLP during 2008.

[34] Year-to-year differences in CloudSat and CALIOP summer cloud fraction profiles over the Pacific marginal seas were also consistent with year-to-year variability in atmospheric circulation patterns (Figure 8). When compared to 2006 and 2008, 2007 had fewer clouds through most of the atmospheric column (0.72 to ~9 km) detected by the merged CloudSat + CALIOP data in the Beaufort Sea, the Chukchi Sea, and the East Siberian Sea (in declining order of magnitude). CALIOP VFM cloud fraction profiles revealed that 2007 also had reduced near-surface cloud

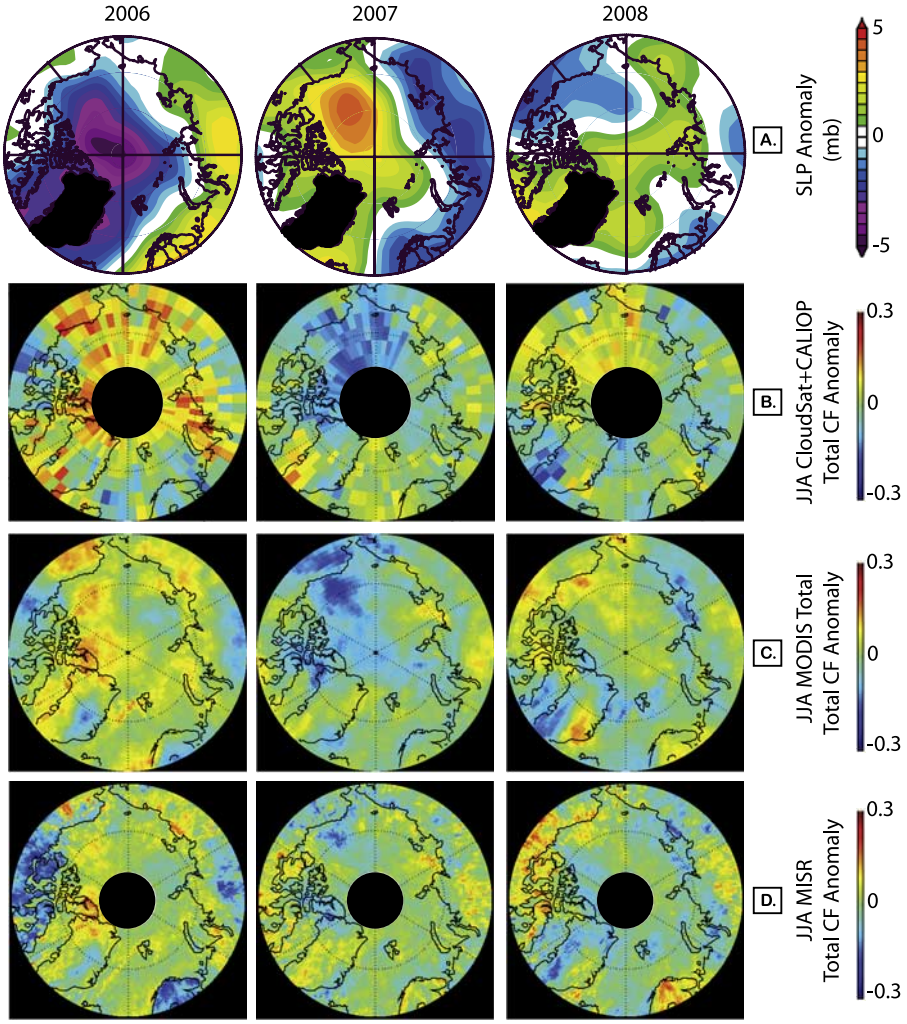

Figure 7. JJA circulation and total cloud pattern anomalies from 2006 to 2008. (a) NRA sea level pressure anomaly. (b) CloudSat + CALIOP total cloud fraction anomaly. Columns are cloudy if the total cloud thickness detected by CloudSat + CALIOP exceeds 960 m (4 bins). (c) MODIS total cloud fraction anomaly. (d) MISR total cloud fraction anomaly. All anomalies are calculated as the difference between the year and the 2006–2008 average.

fractions (<0.72 km) in the Chukchi and Beaufort Seas, but that 2007 and 2008 had similar cloud amounts in the East Siberian Sea.

[35] Summer cloud distributions had a strong spatial association with the Atlantic sector sea ice edge, but a weak spatial association with the Pacific sector sea ice edge. For example, both MISR and MODIS data show little spatial association between total cloud amounts and newly open water in the Pacific sector during July 2007, a month in which significant Arctic sea ice extent loss occurred (Figure 9). Monthly averaged AIRS data from July 2007 show high static stability over the marginal seas in the Pacific sector, which could have suppressed atmosphere-ocean coupling. The lack of spatial association between ice extent and cloudiness in the Pacific marginal seas was also evident during 2006 and 2008, but the atmospheric and sea ice conditions during July 2007 provide the most obvious connection between high static stability and the lack of a summer cloud response to sea ice loss.

[36] CloudSat and CALIOP cloud fraction profiles composited by sea ice presence (Figure 10) allow investigation of the influence of open water on summer cloud profiles. Because only three years of data are included, the composited cloud profiles are a convolution of year-to-year variability in sea ice cover and large-scale atmospheric circulation patterns. In all three Pacific marginal seas, there were fewer clouds over sea ice than over open water. The first-order explanation of this difference is that cloud reductions in 2007 primarily occurred over sea ice. Over the Beaufort Sea, another contributing factor was that 2008 had more open water and more clouds than 2007. Over the Chukchi Sea, a greater percentage of the 2007 cloud reductions occurred over open water than over the Beaufort Sea. As a result, the contrast between ice-covered and open water cloudiness composites resulting from the 2007 cloud reductions was evident, but muted when compared to the Beaufort Sea. Over the East Siberian Sea, there were more (fewer) clouds over open water than over sea ice from 0.5 to 4 km (4 to 8 km).

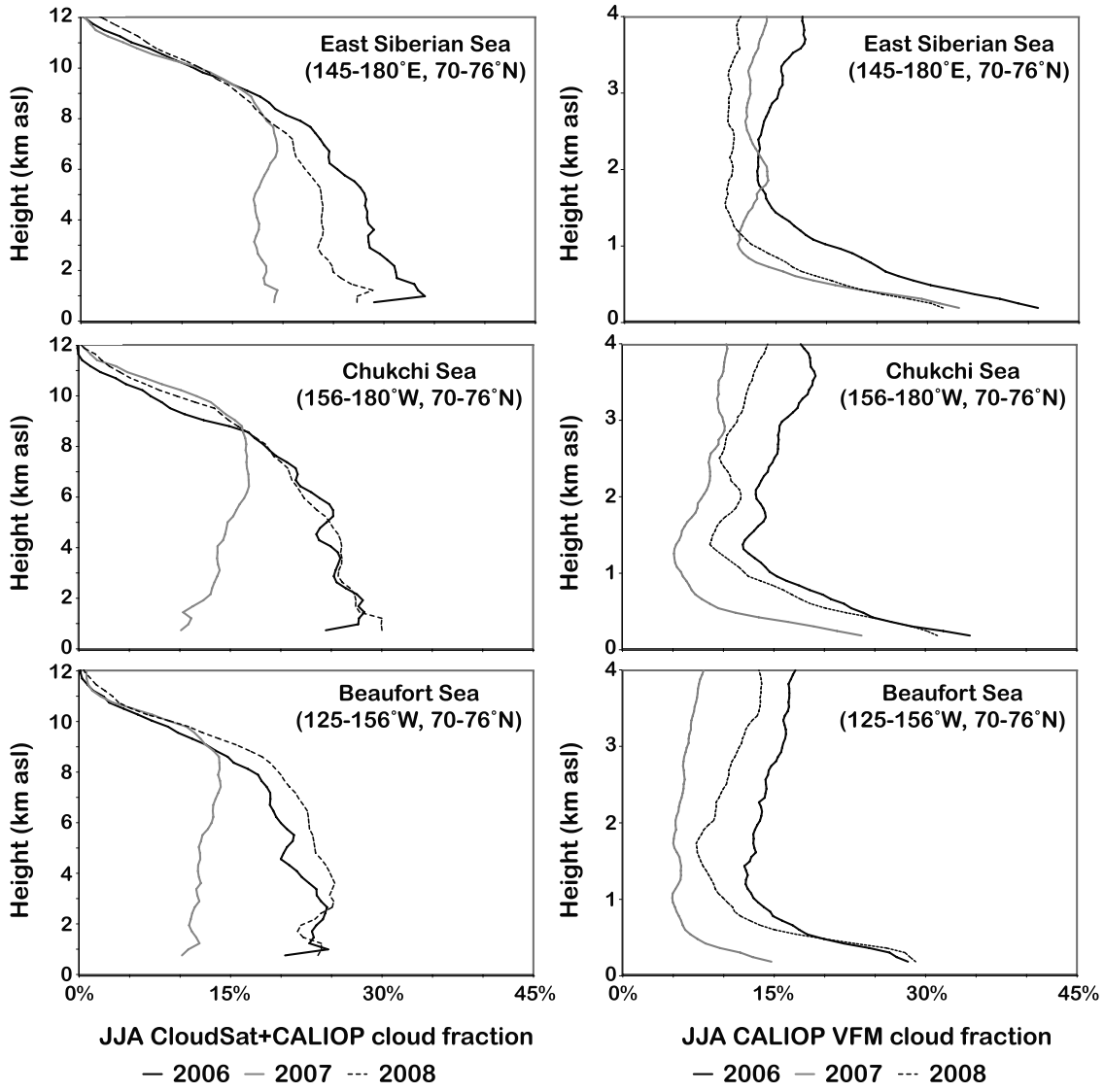

Figure 8. Year-to-year variability in summer CloudSat + CALIOP (radar + lidar) and CALIOP VFM (lidar only) cloud fraction profiles over three Pacific marginal seas.

This compositing relationship resulted because the East Siberian Sea had more clouds over open water during 2007, but fewer mid-level clouds over open water than over sea ice during 2008.

[37] Near the surface, CloudSat and CALIOP cloud fraction profiles composited by sea ice cover show more clouds over open water than over sea ice. The one exception is that CALIOP VFM profiles hint at more clouds over ice in the East Siberian Sea below 500 m. At first, these compositing results may seem incompatible with the poor spatial association between summer cloud cover and sea ice presence shown by MISR and MODIS (Figure 9); however, more low cloud over open water than over sea ice in composited profiles is consistent with the changing large-scale atmospheric conditions. In general, low cloud amounts change more than middle or high cloud amounts in association with SLP variability (e.g., Figure 8). Thus the tendency for 2006–2008 atmospheric circulation patterns to result in low SLP (high SLP) over open water (sea ice) can explain the observed tendency for there to be more low clouds over open water than over sea ice.

3.4. Early Fall (SO) Year-to-Year Variability

3.4.1. Atmospheric and Sea Ice Conditions During Early Fall

[38] Significant year-to-year variability in early fall large-scale circulation patterns occurred from 2006 through 2008 (Figure 1, Figure 2, Figure 11). In the Pacific sector, both 2006 and 2007 had high pressure centered over the Beaufort Sea and low pressure over Bering Straight. 2007 had an extremely strong Beaufort High with low pressure surrounding it on all sides except the Canadian Archipelago. Unlike 2006 and 2007, 2008 had high pressure over the entire Pacific sector. In the Atlantic sector, the 2006 North Atlantic storm track was relatively quiet with the lowest pressures occurring over Northern Russia and the Kara Sea. The 2007 North Atlantic storm track was more active than 2006 and extended very far North into the Arctic, with the lowest pressure

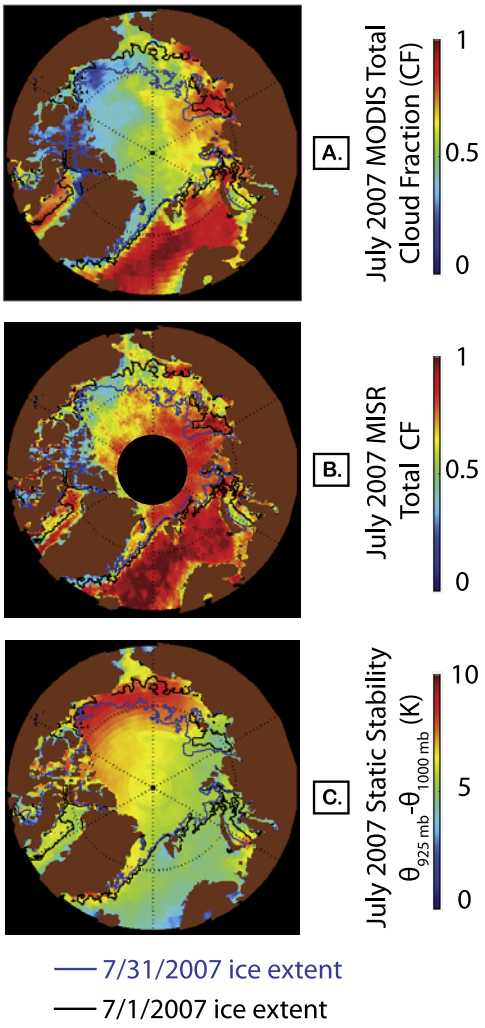

Figure 9. July 2007 clouds, sea ice, and static stability. (a) MODIS total cloud fraction. (b) MISR total cloud fraction. (c) AIRS static stability. AMSR-E 15% ice concentration line is contoured for 1 and 31 July.

centered southeast of Svalbard. The 2008 North Atlantic storm track was confined to the Norwegian Sea, much further South than in 2007.

[39] Early fall sea ice extent was a function of both the summer ice extent loss and early fall atmospheric conditions. At the seasonal minimum in sea ice extent, 2006 had much greater ice coverage than 2007 or 2008; however, by the end of October, 2006 and 2008 had similar ice extents while 2007 still had open water in the Chukchi Sea. Southerly winds along the dateline during 2007 helped delay ice extent recovery and demonstrate the importance of fall atmospheric conditions to fall sea ice formation.

[40] During early fall, surface conditions and the large-scale atmospheric circulation both had a discernable influence on near-surface air temperature structure. The strong association between AIRS 1000 mb air temperatures and sea ice extent reveals that heat lost from the surface ocean to the atmosphere increased surface air temperatures (Figure 12a). The large-scale circulation affected near-surface air temperature structure by controlling heat advection into the Arctic. AIRS observations in the East Siberian Sea show that ocean-to-atmosphere heat transfer and heat advection have competitive influences on near-surface static stability (Figure 12b). During September 2007, static stability was relatively low over the East Siberian Sea because the surface air temperature increases from ocean heat loss was larger than the warming aloft resulting from advection. Conversely, during September 2008, near-surface static stability was relatively high because advection warming aloft was stronger than surface air warming from ocean heat loss.

3.4.2. Cloud Patterns and Vertical Structures During Early Fall

[41] Year-to-year variations in early fall cloud patterns were controlled both by the large-scale circulation and by sea ice extent. Similar to the summer, early fall cloud patterns reflected SLP patterns. For example, there were relatively few clouds under the strong Beaufort High in September 2007 when compared to 2006 and 2008 (Figure 12). Unlike summer (Figure 9), both MODIS and MISR revealed a strong

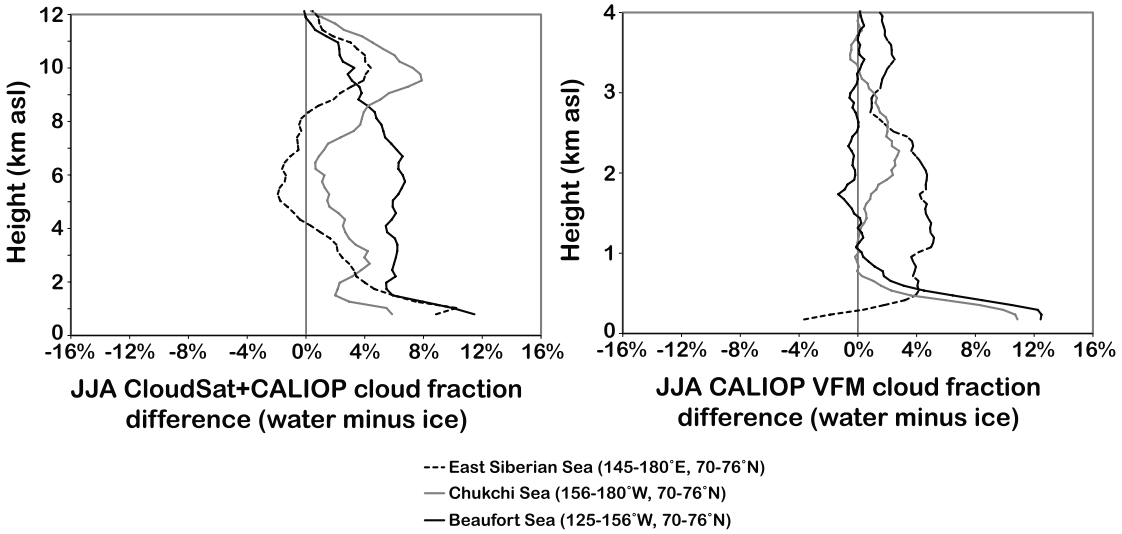

Figure 10. Difference in summer cloud fraction profiles over open water and over sea ice from CloudSat + CALIOP (radar + lidar) and CALIOP VFM (lidar only) data. Compositing was done using AMSR-E observations: water is 0–20% sea ice concentration and ice is 80–100% sea ice concentration.

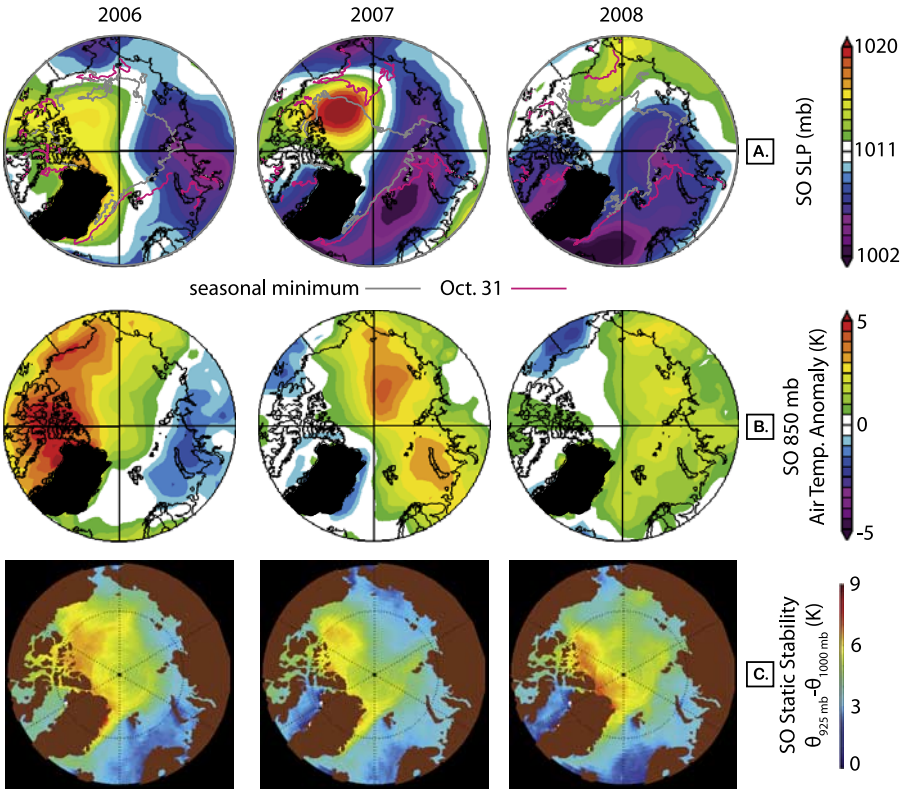

Figure 11. Early fall atmospheric circulation patterns from 2006 to 2008. (a) NRA sea level pressure with seasonal minimum (14 September 2006, 16 September 2007, 14 September 2008) and 31 October AMSR-E 15% ice concentration line. (b) NRA 850 mb air temperature anomaly (from 1979–1995 mean). (c) AIRS near-surface static stability.

association between the sea ice edge and September cloud patterns throughout the Arctic (Figure 12). Cloud cover increased over newly open water in the Pacific sector (i.e., in areas that were covered by ice in previous Septembers). Although the MODIS and MISR cloud distributions were primarily associated with the presence or absence of sea ice, lower tropospheric static stability may have a secondary influence on cloud patterns. For example, the MODIS and MISR data hint that increased static stability during 2008 may have suppressed cloud cover over the East Siberian Sea.

[42] CloudSat + CALIOP and CALIOP VFM cloud fraction profiles over the Pacific marginal seas showed more clouds in early fall than in summer, free tropospheric cloud changes associated with SLP variability, and low-level cloud increases during years with low sea ice extent (Figure 13). Summer-to-fall cloud increases were especially large below 2 km (compare Figure 8 and Figure 13, note different *x* axis scaling). Over the Beaufort and Chukchi Seas, free tropospheric cloudiness was reduced under the strong Beaufort High in early fall 2007. During early fall 2008, the Chukchi Sea had relatively few free tropospheric clouds under a high-pressure ridge. With the exception of the East Siberian Sea in 2008, all three regions had more early fall clouds at low levels in 2007 and 2008 than in 2006 in both the merged CloudSat + CALIOP data set and the CALIOP VFM data set. 2007 had especially large low cloud amounts in the East Siberian and Chukchi Seas, while 2008 had especially large low cloud amounts in the Chukchi and Beaufort Seas. There were also hints of a deepening boundary layer in the Chukchi Sea during 2007 and 2008 and in the East Siberian Sea during 2007. The presence of increased low-level cloud amounts in the combined CloudSat + CALIOP and CALIOP-only profiles during years with low sea ice extent is consistent with the strong spatial association between cloud cover and the sea ice margin seen in MODIS and MISR data (Figure 12).

[43] Combined CloudSat + CALIOP and CALIOP-only cloud fraction profiles composited by sea ice presence provide additional evidence that year-to-year variability in early fall cloudiness was controlled both by year-to-year variability in atmospheric conditions and by sea ice cover (Figure 14). Unlike the summer profiles, the early fall profiles support a relationship between low cloud cover and sea ice that is independent of large-scale circulation masking: mid-level (~2 to 7 km) cloudiness decreased while low-level (<2 km) cloudiness increased. In other words, low cloud changes did not mirror changes in free-tropospheric cloudiness suggesting that they were not linked to the large-scale circulation. Early fall low cloud increases over open water were especially evident over the Chukchi Sea, but were also present over the East Siberian Sea and the Beaufort Sea. Unlike the low cloud increases, mid-level cloud reductions over open water can be explained by masking due to covarying sea ice and large-scale atmospheric conditions. For example, 2006 had more mid-level clouds and more extensive sea ice in the Chukchi Sea, while 2007 and 2008 had fewer midlevel clouds and less extensive

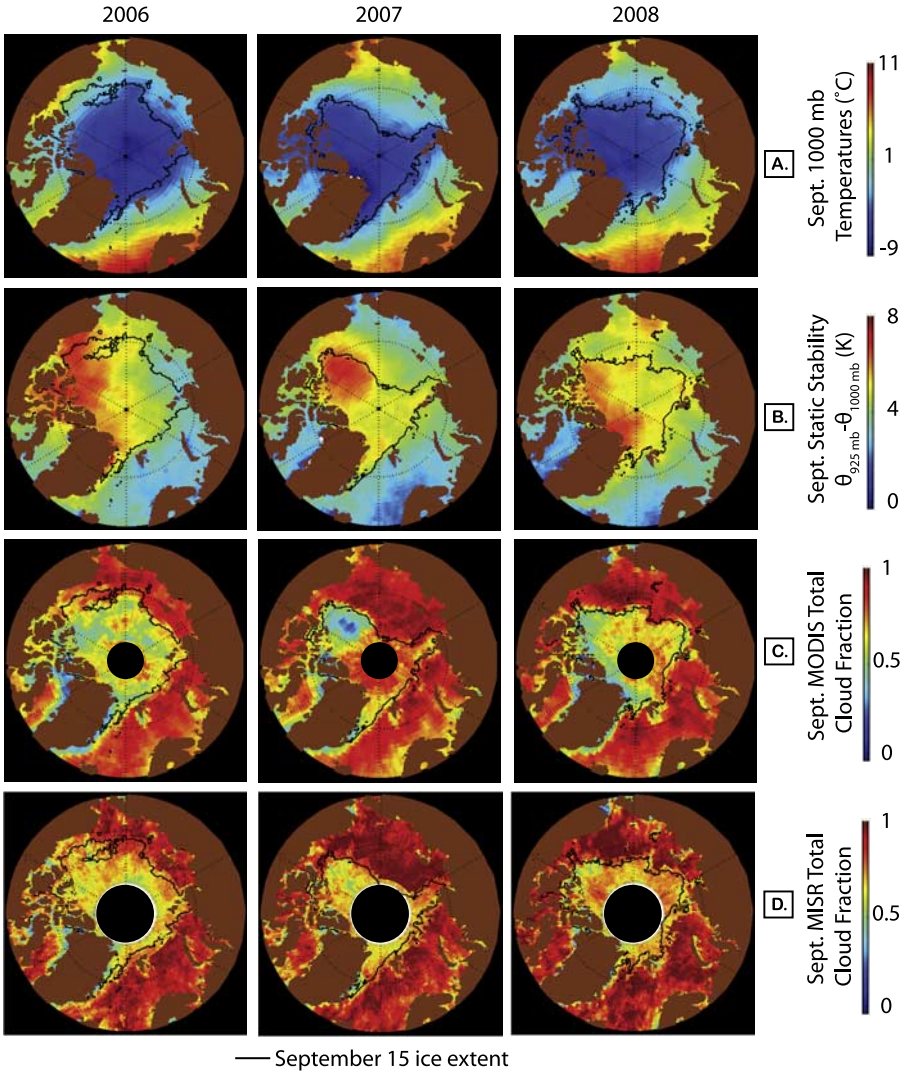

Figure 12. September clouds, sea ice, and static stability from 2006 to 2008. (a) AIRS 1000 mb temperatures with 15 September AMSR-E 15% ice concentration contour. (b) AIRS near-surface static stability. (c) MODIS cloud fraction with 15 September sea ice extent contour. (d) MISR cloud fraction with 15 September sea ice extent contour.

sea ice (Figure 11, Figure 13). These relationships explain why the Chukchi Sea has reduced mid-level cloud over open water (Figure 14), and highlight the difficulty of compositing a short data record to isolate the cloud response to sea ice loss.

4. Discussion

[44] Documenting the influence of large-scale atmospheric circulation patterns on Arctic cloud structure during recent periods of sea ice loss was useful, but not scientifically surprising. Subsidence associated with high-pressure anomalies reduced cloud cover, while ascent associated with low-pressure anomalies increased cloud cover. During summer, cloud changes resulting from large-scale atmospheric circulation variability were evident through most of the atmospheric column including near the surface. This finding contradicts earlier work that suggests that Arctic low clouds are relatively insensitive to the large-scale atmospheric circulation [*Curry et al.*, 1996]. We did not find obvious evidence for a frontal cloud response to newly open water. Changes in cloudiness associated with the large-scale atmospheric circulation were essential to isolate because they imprinted themselves on the differences between cloud vertical structure over sea ice and open water. In other words, understanding the large-scale atmospheric circulation variability and its effect on clouds was critical for identifying the low cloud response to sea ice loss.

[45] The most interesting finding from this study is that the observed low cloud response to Arctic sea ice loss changes through the melt season. While newly open water had little impact on summer cloud presence, low cloud amounts increased over newly open water during early fall. This seasonal shift in the cloud response to sea ice loss occurs because air-sea temperature gradients and near-surface static stability regulate the strength of atmosphere-ocean coupling in the Arctic. During summer, large near-surface static stability and weak air-sea temperature gradients limit turbu-

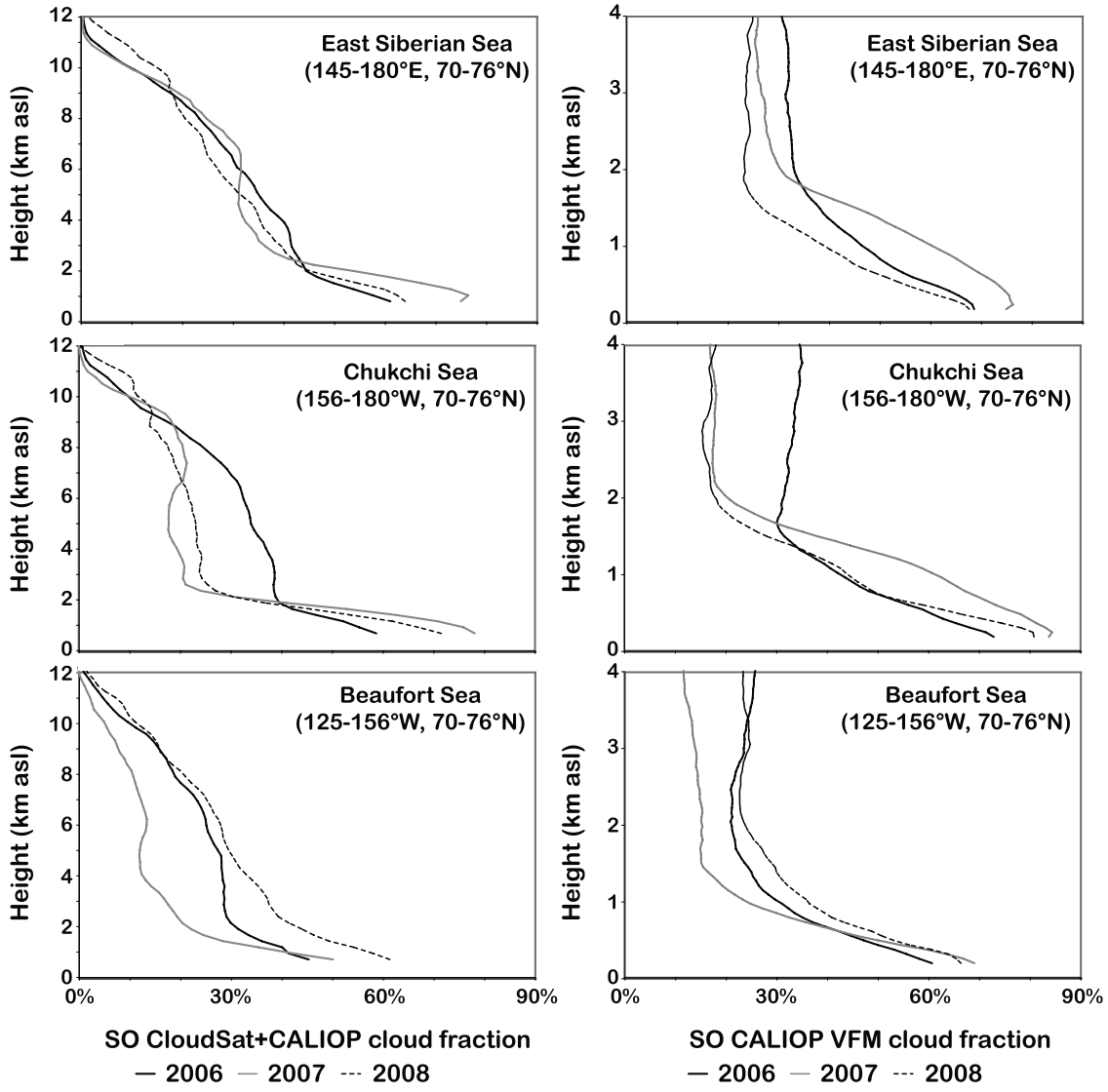

Figure 13. Year-to-year variability in early fall CloudSat + CALIOP (radar + lidar) and CALIOP VFM (lidar only) cloud fraction profiles over three Pacific marginal seas.

lent fluxes, and thus the air-sea interactions that would lead to increased low cloud formation over open water. During early fall, static stability decreases, air-sea temperature gradients increase, and thus turbulent transfer of heat and moisture promotes low cloud formation over newly open water.

[46] This previously undocumented seasonal shift in the cloud response to sea ice loss has significant implications for feedbacks associated with sea ice loss. During summer, clouds regulate the strength of the ice-albedo feedback that accelerates seasonal sea ice loss. When summer cloudiness decreases (increases), more (less) solar radiation reaches the Arctic surface, and the ice-albedo feedback and sea ice loss are enhanced (reduced). Because the large-scale circulation primarily governs summer cloud variability, clouds can either enhance or reduce the ice-albedo feedback. In contrast, the early fall cloud response to sea ice loss, i.e., low clouds forming over newly open water, may enable an early fall cloud-ice feedback. In this study, we identify the potential for an early fall cloud-ice feedback on sea ice extent, but have not quantified its sign or its importance. By September, the SHEBA-observed radiative influence of clouds is to warm the surface [*Intrieri et al.*, 2002], but the net effect of a cloud increase on early fall radiation budgets is a strong function of latitude, time, and surface albedo.

[47] The 2007 melt season provides a stunning example of the ability of clouds to accentuate seasonal sea ice loss. During the 2007 melt season, the largest monthly sea ice extent loss on record occurred from June to July, suggesting that ice-albedo feedbacks played an important role in the record ice loss. Summer 2007 cloud reductions enhanced ice-albedo feedbacks by permitting more solar radiation to reach the surface. Mechanisms for the summer cloud reductions include both subsidence under the strong Beaufort High and advection of warm and dry air along strong SLP gradients. Warm air advection promotes strong temperature inversions by limiting turbulent fluxes and buoyancy-driven cloud formation. Dry air reduces cloud amounts because the critical relative humidity for cloud formation is not as easily reached. During early fall 2007, low cloud increases over newly open water also may have affected sea ice. Early sea

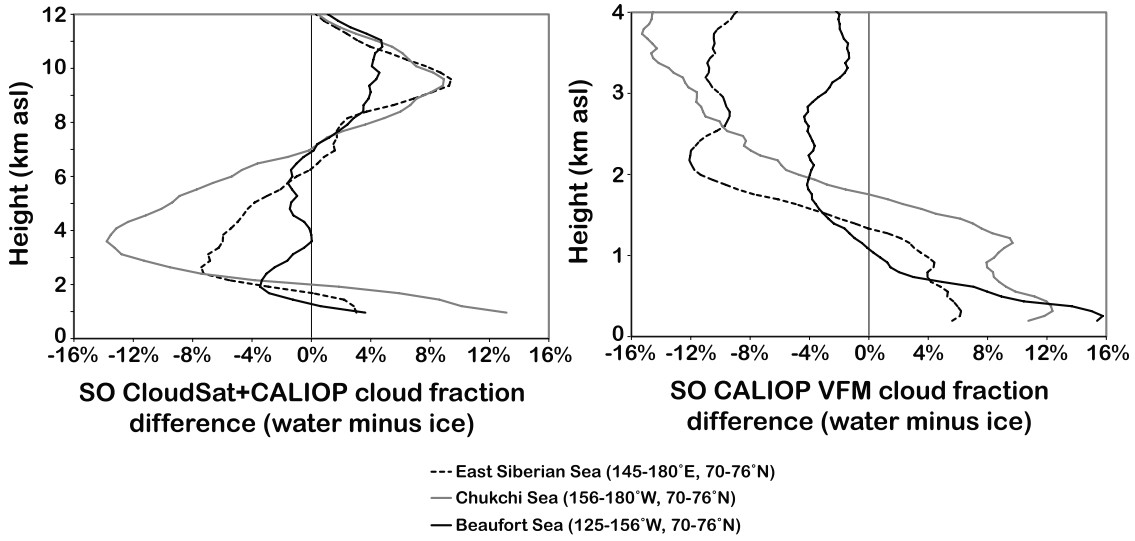

Figure 14. Difference in early fall cloud fraction profiles over open water and over sea ice from CloudSat + CALIOP (radar + lidar) and CALIOP VFM (lidar only) data. Compositing was done using AMSR-E observations: water is 0–20% sea ice concentration and ice is 80–100% sea ice concentration.

ice loss during 2007 promoted increased absorption of solar radiation and large positive sea surface temperature anomalies during early fall. When the surface ocean heat was released back to the lower atmosphere, it reduced static stability and enabled large turbulent fluxes.

[48] The observational results presented here differ from a recently published paper on fall cloud response to sea ice loss. *Schweiger et al.* [2008] (hereafter S08) documented relationships between sea ice extent and fall cloud structure in the ERA-40 reanalysis and TOVS satellite observations. By compositing ERA-40 reanalysis data from 1964 to 2001, S08 found less low-level cloud (1000 to 800 mb, surface to ~1.9 km) and more mid-level cloud (800 to 450 mb, ~1.9 km to 6.1 km) over open water than over sea ice. S08's compositing also revealed more ''upper level'' cloud (<800 mb, above ~1.9 km) over open water than over sea ice in TOVS data available from 1980 to 2004. S08 explain the cloud height increase using ERA-40 static stability composites: the atmosphere overlying sea-ice covered areas had greater static stability and thus lower boundary layer heights than the atmosphere overlying open water areas. Low-level cloud decreased because the temperature increases outpaced moisture increases. In contrast to S08, this study found more low-level cloud (<2 km) and less midlevel cloud (2 to 7 km) in the CloudSat + CALIOP and CALIOP VFM profiles over newly open water (Figure 13, Figure 14). While low-level cloud increases were attributed to sea ice loss, mid-level cloud decreases were attributed to atmospheric circulation pattern variability. No doubt the inconsistency between the fall cloud response in TOVS and ERA-40, and the results presented here should be further explored.

[49] Compared to S08, this study relies on a short time period to examine cloud and sea ice relationships. As a result, the influence of year-to-year variability in atmospheric circulation patterns on clouds must be isolated. Despite this complication, this study focuses on a time period with significantly more seasonal sea ice loss than the S08 time period (Figure 1). Thus important sea ice-cloud relationships should be evident.

[50] Discrepancies between this study and S08 are more likely explained by the different data sets that were used. Given that cloud and boundary layer processes in reanalysis products are largely unconstrained by observations, it is not hard to argue that direct observations should be trusted over the S08 ERA-40 results. It is quite possible that the ERA-40 fall cloud response results from a poorly constrained boundary layer parameterization. Vertical resolution and cloud discrimination are also data set attributes to consider when comparing the assessed cloud response. CloudSat and CALIOP have higher vertical resolution (240 m, 60 m) and better vertical discrimination of cloud amount than the ERA-40 or TOVS data sets analyzed in S08.

[51] The key strength of this analysis is that consistent relationships between cloud, sea ice, and atmospheric circulation patterns are found using four independent satellite data sets during a period that includes the two lowest sea ice extent years on record. Given the substantial retrieval differences, it is encouraging that CloudSat + CALIOP, CALIOP-only, MODIS, and MISR data sets show similar relationships. The fall cloud response results are also consistent with positive cloud anomalies in early Fall 2007 observed by AVHRR [*Levinson and Lawrimore*, 2008]. Despite the confidence gained from consistency between multiple independent data sets, additional observations are needed. Polar cloud retrievals based on passive instruments should be taken with caution. For example, the spatial association of the clouds and the sea ice margin in September looks suspiciously strong (Figure 12); however, the lack of such association in the equivalent July retrievals is reassuring (Figure 9). Although the cloud profiles from CloudSat + CALIOP provide new insights into the vertical structure of cloud variability in the Arctic, their relatively poor spatial sampling, short data record, lack of data poleward of 82 N, and difficulty with cloud identification due to attenuation and surface clutter limit their utility in

assessing relationships between cloud, circulation, and sea ice changes.

5. Summary

[52] In this study, ocean and atmospheric observations and the NCEP/NCAR atmospheric reanalysis were used to document the physical controls on Arctic clouds from 2006 to 2008, a time period over which unprecedented summer and early fall Arctic sea ice extent loss occurred. The primary findings are:

[53] 1. Interannual variability in large-scale atmospheric circulation patterns and surface conditions explain variability in Arctic cloud presence and vertical structure. Clouds are intimately tied to large-scale atmospheric circulation patterns, but near-surface static stability and surface cover (sea ice or open water) can exert significant control on low cloud presence.

[54] 2. During summer, year-to-year variability in Arctic cloudiness is controlled by year-to-year variability in large-scale atmospheric circulation patterns. We found no observational evidence for a cloud response to sea ice loss during summer. We attribute this lack of a summer cloud response to inversions and weak air-sea temperature gradients that limit atmosphere-ocean coupling through turbulent fluxes.

[55] 3. During early fall, year-to-year variability in Arctic cloudiness is controlled both by year-to-year variability in the large-scale atmospheric conditions and by year-to-year variability in the sea ice edge. In contrast to summer, low-level cloud amounts (<2 km) increased over newly open water in the Pacific sector. This early fall cloud response to sea ice loss is enabled by relatively low near-surface static stability, strong air-sea temperature gradients, and turbulent vertical transfer of moisture from the ice-free ocean. Low-level cloud increases associated with open water could contribute to an early fall cloud-ice feedback.

[56] 4. Clouds and winds combined to enhance sea ice loss throughout the 2007 melt season. Summer cloud reductions associated with a strong Beaufort High enhanced ice-albedo feedbacks, while fall cloud increases over newly open water helped trap heat by increasing downwelling longwave radiation but also reduced net absorbed shortwave radiation.

[57] We neglect many aspects of the cloud influence on and response to sea ice loss. First, understanding changes in cloud macrophysical and microphysical properties is essential for quantifying the influence of clouds on sea ice loss. In future work, we will assess both changes in cloud properties (e.g., thickness, water content, and particle size) and the impact of cloud variations on radiative fluxes. We also plan to use the observed seasonal timing of cloud response to sea ice loss as a critical test of the model cloud and boundary layer parameterizations. Only through careful evaluation of models and observations will we understand the influence of clouds on our present trajectory toward a seasonally sea ice-free Arctic.

[58] **Acknowledgments.** We thank Chris O'Dell for processing and helping interpret MODIS data, Larry Di Girolamo and Alexander Menzies for processing and helping interpret MISR data, and Clara Deser, Hugh Morrison, Kevin Trenberth, and Gijs de Boer for fruitful discussions and constructive feedback. This work was funded by the NASA CloudSat project (NAS5-99237). Additional support was provided by the National Center for Atmospheric Research, which is funded by the United States National Science Foundation.

References

Ackerman, S. A., R. E. Holz, R. Frey, E. W. Eloranta, B. C. Maddux, and M. McGill (2008), Cloud detection with MODIS: Part II. Validation, *J. Atmos. Oceanic Technol.*, *25*(7), 1073–1086.

Alexander, M. A., U. S. Bhatt, J. E. Walsh, M. S. Timlin, J. S. Miller, and J. D. Scott (2004), The atmospheric response to realistic Arctic sea ice anomalies in an AGCM during winter, *J. Clim.*, *17*(5), 890–905.

Bodas-Salcedo, A., M. J. Webb, M. E. Brooks, M. A. Ringer, K. D. Williams, S. F. Milton, and D. R. Wilson (2008), Evaluating cloud systems in the Met Office global forecast model using simulated CloudSat radar reflectivities, *J. Geophys. Res.*, *113*, D00A13, doi:10.1029/2007JD009620.

Brummer, B. (1996), Boundary-layer modification in wintertime cold-air outbreaks from Arctic sea ice, *Boundary Layer Meteorol.*, *80*, 109–125.

Cavalieri, D., C. Parkinson, P. Gloersen, and H. J. Zwally (1996), Sea Ice Concentrations From Nimbus-7 SMMR and DMSP SSM/I Passive Microwave Data, 1979–2008, http://nsidc.org/data/nsidc-0051.html, Natl. Snow and Ice Data Cent., Boulder, Colo. (Updated 2008)

Cavalieri, D., T. Markus, and J. Comiso (2004), AMSR-E/Aqua Daily L3 12.5 km Brightness Temperature, Sea Ice Concentration, and Snow Depth Polar Grids V002, 2006–2008, http://nsidc.org/data/ae_si12.html, Natl. Snow and Ice Data Cent., Boulder, Colo. (Updated daily)

Curry, J. A., W. B. Rossow, D. Randall, and J. L. Schramm (1996), Overview of arctic cloud and radiation characteristics, *J. Clim.*, *9*, 1731–1764.

de Boer, G., E. Eloranta, and M. Shupe (2009), Arctic mixed-phase stratiform cloud properties from multiple years of surface-based measurements at two high-latitude locations, *J. Atmos. Sci.*, in press.

Deser, C., J. E. Walsh, and M. S. Timlin (2000), Arctic sea ice variability in the context of recent atmospheric circulation trends, *J. Clim.*, *13*, 617–633.

Deser, C., G. Magnusdottir, R. Saravanan, and A. Phillips (2004), The effects of North Atlantic SST and sea ice anomalies on the winter circulation in CCM3: Part II. Direct and indirect components of the response, *J. Clim.*, *17*(10), 877–899.

Deser, C., R. Tomas, M. Alexander, and D. Lawrence (2009), The seasonal atmospheric response to projected Arctic Sea ice loss in the late 21st century, *J. Clim.*, in press.

Di Girolamo, L., and W. J. Wilson (2003), A first look at band-differenced angular signatures for cloud detection from MISR, *IEEE Trans. Geosci. Remote Sens.*, *41*, 1730–1734.

Di Girolamo, L., A. Menzies, G. Zhao, and D. J. Diner (2009), Multi-angle Imaging SpectroRadiometer cloud fraction by altitude algorithm theoretical basis, *JPL Tech. Doc. D-62358*, Jet Propul. Lab., Calif. Inst. of Technol. Pasadena, Calif., 19 pp.

Divakarla, M. G., C. D. Barnet, M. D. Goldberg, L. M. McMillin, E. Maddy, W. Wolf, L. Zhou, and X. Liu (2006), Validation of AIRS temperature and water vapor retrievals with matched radiosonde observations and forecasts, *J. Geophys. Res.*, *111*, D09S15, doi:10.1029/2005JD006116.

Gettelman, A., V. P. Walden, L. M. Miloshevich, W. L. Roth, and B. Halter (2006), Relative humidity over Antarctica from radiosondes, satellites and a general circulation model, *J. Geophys. Res.*, *111*, D09513, doi:10.1029/2005JD006636.

Herman, G. F., and R. Goody (1976), Formation and persistence of summertime Arctic stratus clouds, *J. Atmos. Sci.*, *33*, 1537–1553.

Higgins, M. E., and J. J. Cassano (2009), Impacts of reduced sea ice on winter Arctic atmospheric circulation, precipitation, and temperature, *J. Geophys. Res.*, *114*, D16107, doi:10.1029/2009JD011884.

Hurrell, J., J. J. Hack, D. Shea, J. M. Caron, and J. Rosinski (2008), A new sea surface temperature and sea ice boundary data set for the Community Atmosphere Model, *J. Clim.*, *21*(19), 5145–5153.

Intrieri, J. M., C. W. Fairall, M. D. Shupe, P. O. G. Persson, E. L. Andreas, P. S. Guest, and R. E. Moritz (2002), An annual cycle of Arctic surface cloud forcing at SHEBA, *J. Geophys. Res.*, *107*(C10), 8039, doi:10.1029/2000JC000439.

Kalnay, E., et al. (1996), The NCEP/NCAR Reanalysis 40-year Project, *Bull. Am. Meteorol. Soc.*, *77*, 437–471.

Kay, J. E., T. L'Ecuyer, A. Gettelman, G. Stephens, and C. O'Dell (2008), The contribution of cloud and radiation anomalies to the 2007 Arctic sea ice extent minimum, *Geophys. Res. Lett.*, *35*, L08503, doi:10.1029/2008GL033451.

Klein, S. A., and D. L. Hartmann (1993), The seasonal cycle of low stratiform clouds, *J. Clim.*, *6*(8), 1587–1606.

Klein, S. A., et al. (2009), Intercomparison of model simulations of mixed-phase clouds observed during the ARM Mixed-Phase Arctic Cloud Experiment: Part I. Single-layer cloud, *Q. J. R. Meteorol. Soc.*, *641*, 979–1002, doi:10.1002/qj.416.

Levinson, D. H., and J. J. Lawrimore (Ed.) (2008), The state of the climate in 2007, *Spec. Suppl. Bull. Am. Meteorol. Soc.*, *89*(7), 181 pp.

L'Heureux, M. L., A. Kumar, G. D. Bell, M. S. Halpert, and R. W. Higgins (2008), Role of the Pacific-North American (PNA) pattern in the 2007 Arctic sea ice decline, *Geophys. Res. Lett.*, *35*, L20701, doi:10.1029/2008GL035205.

Liu, A. Q., G. W. K. Moore, K. Tsuboki, and I. A. Renfrew (2006), The effect of the sea-ice zone on the development of boundary-layer role clouds during cold air outbreaks, *Boundary Layer Meteorol.*, *118*, 557–581.

Mace, G. G., Q. Zhang, M. Vaughan, R. Marchand, G. Stephens, C. Trepte, and D. Winker (2009), A description of hydrometeor layer occurrence statistics derived from the first year of merged Cloudsat and CALIPSO data, *J. Geophys. Res.*, *114*, D00A26, doi:10.1029/2007JD009755.

Marchand, R., G. G. Mace, T. Ackerman, and G. Stephens (2008), Hydrometeor detection using Cloudsat—An earth-orbiting 94-GHz cloud radar, *J. Atmos. Oceanic Technol.*, *25*(4), 519–533.

Meier, W., F. Fetterer, K. Knowles, M. Savoie, and M. J. Brodzik (2006), Sea Ice Concentrations From Nimbus-7 SMMR and DMSP SSM/I Passive Microwave Data, 1979–2008, http://nsidc.org/data/nsidc-0051.html, Natl. Snow and Ice Data Cent., Boulder, Colo. (Updated quarterly)

Moroney, C., R. Davies, and J.-P. Muller (2002), Operational retrieval of cloud-top heights using MISR data, *IEEE Trans. Geosci. Remote Sens.*, *40*, 1532–1540.

Morrison, H., and J. O. Pinto (2005), Mesoscale modeling of Springtime Arctic mixed-phase stratiform clouds using a new two-moment bulk microphysics scheme, *J. Atmos. Sci.*, *62*, 3683–3702.

Ogi, M., and J. M. Wallace (2007), Summer minimum Arctic sea ice extent and the associated summer atmospheric circulation, *Geophys. Res. Lett.*, *34*, L12705, doi:10.1029/2007GL029897.

Paluch, I. R., D. H. Lenschow, and Q. Wang (1997), Arctic boundary layer in the fall season over open and frozen sea, *J. Geophys. Res.*, *102*(D22), 25,955–25,971.

Perovich, D. K., J. A. Richter-Menge, K. F. Jones, and B. Light (2008), Sunlight, water, and ice: Extreme Arctic sea ice melt during the summer of 2007, *Geophys. Res. Lett.*, *35*, L11501, doi:10.1029/2008GL034007.

Pinto, J. O. (1998), Autumnal mixed-phase cloudy boundary layers in the Arctic, *J. Atmos. Sci.*, *55*, 2016–2038.

Platnick, S., M. D. King, S. A. Ackerman, W. P. Menzel, B. A. Baum, J. C. Riedi, and R. A. Frey (2003), The MODIS cloud products: Algorithms and examples from Terra, *IEEE Trans. Geosci. Remote Sens.*, *41*(2), 459–473.

Schweiger, A. J., R. W. Lindsay, S. Vavrus, and J. A. Francis (2008), Relationships between Arctic sea ice and clouds during Autumn, *J. Clim.*, *21*, 4799–4810, doi:10.1175/2008JCLI2156.1.

Serreze, M. C., and A. P. Barrett (2008), The summer cyclone maximum over the Central Arctic Ocean, *J. Clim.*, *21*, 1048–1065.

Serreze, M. C., M. M. Holland, and J. Stroeve (2007), Perspectives on the Arctic's shrinking sea-ice cover, *Science*, *315*(5818), 1533–1536, doi:10.1126/science.1139426.

Stamnes, K., R. G. Ellingson, J. A. Curry, J. E. Walsh, and B. D. Zak (1999), Review of science issues, deployment strategy, and status for the ARM North Slope of Alaska–Adjacent Arctic Ocean Climate Research Site, *J. Clim.*, *12*, 46–63.

Stephens, G. L., et al. (2008), CloudSat mission: Performance and early science after the first year of operation, *J. Geophys. Res.*, *113*, D00A18, doi:10.1029/2008JD009982.

Stroeve, J., M. Serreze, S. Drobot, S. Gearheard, M. Holland, J. Maslanik, W. Meier, and T. Scambos (2008), Arctic sea ice extent plummets in 2007, *Eos Trans. AGU*, *89*(2), doi:10.1029/2008EO020001.

Tsukernik, M., D. N. Kindig, and M. C. Serreze (2007), Characteristics of winter cyclone activity in the northern North Atlantic: Insights from observations and regional modeling, *J. Geophys. Res.*, *112*, D03101, doi:10.1029/2006JD007184.

Walter, B. A. (1980), Wintertime observations of roll clouds in the Bering Sea, *Mon. Weather Rev.*, *108*(12), 2024–2031.

Zhang, J., R. Lindsay, M. Steele, and A. Schweiger (2008), What drove the dramatic retreat of arctic sea ice during summer 2007?, *Geophys. Res. Lett.*, *35*, L11505, doi:10.1029/2008GL034005.

Zhao, G., and L. Di Girolamo (2004), A cloud fraction versus view angle technique for automatic in-scene evaluation of the MISR cloud mask, *J. Appl. Meteorol.*, *43*, 860–869.

A. Gettelman and J. E. Kay, Climate and Global Dynamics, National Center for Atmospheric Research, P.O. Box 3000, Boulder, CO 80307-3000, USA. (jenkay@ucar.edu)